An Enhanced Viscoplastic Constitutive Model for Semi-Solid Materials to Analyze Shear Localization

M.H. Sheikh-Ansari, M. Aghaie-Khafri [*]

Faculty of Materials Science and Engineering, K.N. Toosi University of Technology, Tehran, Iran

ABSTRACT

Semi-solid materials undergo strain localization and shear band formation as a result of granular nature of semi-solid deformation. In the present study, to analyze the shear localization, a unified viscoplastic constitutive model was developed for the homogeneous flow. Then, a linearized analysis of the stability performed by examining the necessary condition for the perturbation growth. For this purpose, a shear layer model was considered to analyze the perturbation growth and subsequent instability. The perturbation analysis revealed that the failure mode in semi-solid materials is diffused with long wave length regime, rather than to be localized and exhibiting short wave length regime. Moreover, decreasing the solid skeleton has a retarding effect on the perturbation growth and localization at low and modest strain rates. The performed analysis showed that the localization analysis results in a new interpretation for the micro-mechanisms of the semi-solid deformation. The constitutive model was fairly well correlated with the experimental results. ©2018 IAU, Arak Branch. All rights reserved.

Keywords : Viscoplastic model; Shear band; Perturbation growth; Dilatancy; Semi-Solid.

1 INTRODUCTION

FORMING in semi-solid state is a promising method, drawn great attention due to its ability to combine the advantages of both conventional casting and forging in order to produce near net shaped components via applying very low forces [1-5]. The impingement of grains occurs above a critical solid fraction, named the dendritic coherency solid fraction (f_s^{coh}), leading to a long range interconnectivity in the force chain network. f_s^{coh} that depends on the solid fraction as well as the shape of envelops at coherency. For equiaxed dendritic microstructure, f_s^{coh} is about 0.15 while for granular ones is about 0.5 [6]. The investigations of Gourlay et al. [7] have demonstrated that the semi-solid materials at high solid fractions, $f_s \geq f_s^{coh}$, with a granular microstructure, deform as a geomaterial, e.g. rock and soil, associated with Reynolds dilatancy. The dilatancy is the main feature of granular materials, defined as the volumetric variation during shearing, leading the grains to move relative to each other. Based on the investigation performed by synchrotron radiography, Fonseca et al. [8] have also revealed that the deformation of a semi-solid alloy with globular morphology at high solid fraction occurs by the granular mechanism. The comprehensive interpretation of the granular features of semi-solid deformation is given by Kareh

et al. [9]. Gourlay and Dahle [6] have revealed that at the solid fraction which is shortly beyond the dendrite coherency, the semi-solid deforms via crystal rearrangement and Reynolds dilatancy, which is an increase in volume due to the shear stresses, causes the deformation to localize into shear bands. In another study, Meylan et al. [10] have shown that dilatant shear bands initiate beyond the peak stress, and the band thickness increases from ~10 to ~16 times of the mean grains thickness during the strain softening stage. On the other hand, the rate-dependency of the semi-solid materials is a critical factor to analyze the instability [11,12]. In the context of rate-independent materials, localization can be assumed as a bifurcation, loss of ellipticity, in the velocity equations of continuing equilibrium [13]. It is commonly studied by a band analysis [13,14]. An alternative approach for analyzing the flow localization of rate-dependent materials was developed by considering an infinitesimal perturbation in a given system and examining the necessary condition for the inhomogeneity growth [15-17].

It is widely accepted that formability can be restricted by the flow localization [18,19]. In a recent study [20], a criterion was developed in order to indicate the flow localization in semi-solid deformation, based on the thermodynamics of large deformation. Objective of the present work is to determine the necessary condition of shear localization in the semi-solid deformation by applying a linear perturbation analysis on a developed viscoplastic constitutive model.

2 CONSTITUTIVE MODEL

The impingement of grains forms a solid skeleton, whose fraction is designated by ψ. At $f_s < f_s^{coh}$, ψ becomes zero and when $f_s = 1$, ψ is unity. For the localization analysis, the condition of perturbation growth in a homogeneous deformation should be considered. In the homogeneous part of the flow curve, the value of ψ remains constant before reaching the peak stress. The solid skeleton breaks beyond the peak stress. The instability indicates with the local decrease of ψ value, leading the solid skeleton to be divided into several blocks. In this case, ψ tends to zero in such localization bands.

By analogy with the formulation used for liquid systems, we have:

$$\tau = 2\eta\dot{\varepsilon}^{vp}, \tag{1}$$

where τ is the effective stress, $\tau = \sqrt{\dfrac{3}{2}s:s}$, where s is the deviatoric part of the stress tensor, η is the viscosity and $\dot{\varepsilon}^{vp}$ is the equivalent viscoplastic strain rate, $\sqrt{\dfrac{2}{3}D^{vp}:D^{vp}}$, where D^{vp} is the viscoplastic part of the rate of deformation, which is the symmetric part of the velocity gradient:

$$D_{ij} = \frac{1}{2}(\frac{\partial v_i}{\partial x_j} + \frac{\partial v_j}{\partial x_i}). \tag{2}$$

The viscosity of a solid material is commonly expressed via the following form:

$$\eta = L(\frac{\sqrt{3}\dot{\varepsilon}_{eq}}{\dot{\gamma}_0})^{m-1}, \tag{3}$$

where L is the consistency, and $\dot{\gamma}_0$ is the reference strain rate. Development of Eq. (3) to take ψ into account results in:

$$\eta = K(\psi)(\frac{\sqrt{3}\dot{\varepsilon}_{eq}}{\dot{\gamma}_0})^{m(\psi)-1}, \tag{4}$$

where $K(\psi)$ is the consistency parameter, defined as a function of ψ. Eq. (4) represents the common solid deformation when ψ is unity, $K(1)$, and when strain-rate sensitivity is also considered, where m defined as in the hot deformation. As the viscous flows of liquids is concerned, $K(0)$ represents the liquid viscosity, η_{liquid}, and m becomes unity. Therefore, linear interpolation equations can be considered to describe the evolution of $K(\psi)$ and m as:

$$K(\psi) = \psi K_{solid} + (1-\psi) K_{liquid}, \tag{5a}$$

$$m(\psi) = 1 + \psi(m_{solid} - 1), \tag{5b}$$

where K_{solid} and K_{liquid} are the consistency parameters for alloy at solid and liquid states, respectively. Due to the presence of the skeleton, the semi-solid material experiences an intense hardening till the stress reaches to a peak value. For modelling purpose, it can be considered as the developed work hardening. Therefore, the inelastic strain can be considered as an internal parameter. By considering Eq. (4), Eq. (1) can be written as:

$$\tau = 2K(\psi)(\frac{\sqrt{3}\dot{\varepsilon}_{eq}}{\dot{\gamma}_0})^{m(\psi)-1} \dot{\varepsilon}^{vp} (\varepsilon^{vp})^{n(\psi)}. \tag{6}$$

where n is the hardening exponent. Furthermore, it can be assumed that variations of stress with strain become linear and the slop of the line decreases by decreasing ψ. This can be attributed to the fact that in such a elasto-viscoplastic deformation, decreasing ψ leads to decrease the role of the viscoplastic deformation of solid bonds, results in a linear behavior at the initial rising part of the stress-strain curve, $n \approx 1$. Considering model development, the variation of n in terms of ψ is assumed to obtain by the following relation:

$$n(\psi) = 1 + \psi(n_{solid} - 1). \tag{7}$$

Note that the value of n_{solid} is very low at such high temperatures. The relative movement of grains and agglomerates needs to overcome the internal friction. Considering the internal friction, Eq. (6) becomes:

$$\tau - \mu(\sigma_h - p_L) = 2K(\psi)(\frac{\sqrt{3}\dot{\varepsilon}_{eq}}{\dot{\gamma}_0})^{m(\psi)-1} \dot{\varepsilon}^{vp} (\varepsilon^{vp})^{n(\psi)}, \tag{8}$$

where μ is the internal friction coefficient, p_L and σ_h are the liquid pore pressure and the hydrostatic part of stress, both of them are developed in the skeleton, and $\sigma_h - p_L$ represents the effective hydrostatic pressure [21]. On the other hand, the normal strain rate is developed as a result of dilatancy, expressed as follows:

$$\dot{\zeta}^{vp} = \beta \dot{\gamma}^{vp}, \tag{9}$$

where β is the value of the dilatancy and $\dot{\gamma}^{vp}$ is the shear strain rate.

3   PERTURBATION ANALYSIS

For simplicity's case, an infinite layer with a normal in the *y* direction, sheared in the plane strain condition, is considered (Fig. 1).
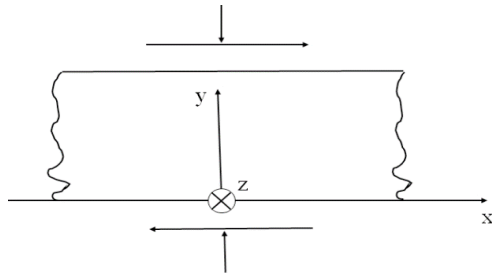
Fig.1
An infinite layer sheared under plain strain condition, in presence of the compressive stress.

The homogeneity of the layer is satisfied in the x and z direction, while a small perturbation exists in the y direction. The perturbation of both shear and normal stresses must be zero in the y direction, i.e. $\tilde{\tau} = \tilde{\sigma}_h = 0$, to satisfy the equilibrium condition. The dilatancy induces a pressure gradient, plays as a driving force for diffusion of the liquid phase. Considering the loading type, the following relation between σ_h, or p_L in undrained condition and τ was considered:

$$\sigma_h = p_L = N\tau, \tag{10}$$

where N is a loading parameter denotes the type of loading. For example, in the pure shearing and simple compression test N is zero and 0.5, respectively. Moreover, a relation between τ and ψ was considered as:

$$\tau = \psi\tau_s, \tag{11}$$

where τ_s represents the shear stress when $\psi = 1$. Therefore, Eq. (10) is rewritten as:

$$\sigma_h = p_L = N\psi\tau_s. \tag{12}$$

The constitutive equation is denoted by Eq. (8), and the assumed perturbation in the linearized form is written as:

$$\frac{\mu\tilde{p}_L}{\tau} = \frac{\tilde{K}(\psi)}{K(\psi)} + m\frac{\dot{\tilde{\gamma}}^{yp}}{\dot{\gamma}^{yp}} + n\frac{\tilde{\gamma}^{yp}}{\gamma^{yp}} + \tilde{m}\ln\dot{\gamma}^{yp} + \tilde{n}\ln\gamma^{yp}. \tag{13}$$

Considering Eqs. (5b) and (7), Eq. (18) reduces to:

$$\frac{\mu\tilde{p}_L}{\tau} = \frac{\tilde{K}(\psi)}{K(\psi)} + m\frac{\dot{\tilde{\gamma}}^{yp}}{\dot{\gamma}^{yp}} + n\frac{\tilde{\gamma}^{yp}}{\gamma^{yp}} - \tilde{\psi}R, \tag{14}$$

where $R = (1-m_s)\ln\dot{\gamma}^{yp} + (1-n_s)\ln\gamma^{yp}$. Inserting Eqs. (5a) and (17) into Eq. (14), and replacing $\dot{\gamma}^{yp}$ with the differentiated form, $\dfrac{d\gamma^{yp}}{dt}$, gives:

$$\frac{d\tilde{\gamma}^{yp}}{d\gamma^{yp}} + \frac{n}{m\gamma^{yp}}\tilde{\gamma} = \frac{\tilde{\psi}\Lambda}{m\tau K(\psi)}. \tag{15}$$

where $\Lambda = [\mu N\tau_s K(\psi) - \tau(K_{solid} - K_{susp}) + R\psi\tau K(\psi)]$. Neglecting the initial perturbation in γ^{yp}, $\tilde{\gamma}(0)$, the solution for the above differential equation is given by:

$$\tilde{\gamma}(\gamma) = \frac{\tilde{\psi}}{mK(\psi)\gamma^{n/m}}\int_0^\gamma \frac{\Lambda(\gamma')^{n/m}}{\tau(\gamma')}d\gamma'. \tag{16}$$

On the other hand, Darcy's law dictates that the fluid content crossing at a unit area in the time unit, M, is a function of the fluid pressure gradient:

$$M = -\chi \nabla p,$$ (17)

where χ is the permeability. Considering conservation of mass law, we have

$$divM + \dot{\zeta} = 0.$$ (18)

Inserting Eq. (17) into Eq. (18) and using Eq. (12), gives:

$$\frac{d\tilde{\zeta}}{dt} = \chi N \tau_s \frac{d^2\tilde{\psi}}{dy^2}.$$ (19)

Moreover, based on the dilatancy relation, Eq. (9), we have:

$$\frac{d\tilde{\zeta}}{dt} = \left\{\frac{\beta}{mK(\psi)(\gamma)^{n/m}} \int_0^\gamma \frac{\Lambda(\gamma')^{n/m}}{\tau(\gamma')} d\gamma'\right\} \frac{d\tilde{\psi}}{dt}.$$ (20)

Eqs. (19) and (20) result in:

$$\frac{d^2\tilde{\psi}}{dy^2} = \left\{\frac{\beta}{\chi N \tau_s mK(\psi)(\gamma)^{n/m}} \int_0^\gamma \frac{\Lambda(\gamma')^{n/m}}{\tau(\gamma')} d\gamma'\right\} \frac{d\tilde{\psi}}{dt}.$$ (21)

Eq. (21) indicates an ordinary diffusion equation. The perturbation growth needs a negative value for the term in the parenthesis. To examine this condition, both m and Λ should be evaluated. Considering $K_s \gg K_L$, and using Eq. (13) the latter term is reduced to $K_s\tau[\mu N - 1 + R\psi^2]$. For a constant positive m, perturbation growth requires $[\mu N - \frac{(\tau - \tau_y)}{\tau} + R\psi^2] < 0$. The first and the second terms are positive and negative, respectively. γ^{yp} is very small at the hardening part of flow curves. Therefore, $\ln \gamma^{yp}$ has a negative value. Moreover, at $\dot{\gamma}^{yp} < e$, where e is a base number approximately equal to 2.718, $\ln \dot{\gamma}^{yp} < 0$. Therefore, R has a negative value at low and modest strain rates. Moreover, the maximum value of N is 0.5, for the compression test. Considering the von-Misses criterion, the maximum value of μ is also 0.577, for the cohesive friction. Therefore, the maximum value of μN is 0.29. It reveals that the expression of $\mu N - 1 + R\psi^2$ is strongly negative at low and modest strain rates. It shows that the condition of perturbation growth is satisfied as soon as the deformation is initiated. This result contradicts the fact that the instability occurs beyond the peak stress. Therefore, it can be concluded that the granular deformation, which is associated with localization, necessitates the breakdown of agglomerates bonds.

By neglecting K_L, the evolution of $\tilde{\gamma}(\gamma)$, time derivative of Eq. (16), is given by:

$$\frac{d\tilde{\gamma}}{dt} = \left\{\frac{1}{m\psi\gamma^{n/m}} \int_0^\gamma \frac{\tau[\mu N - 1 + R\psi^2](\gamma')^{n/m}}{\tau(\gamma')} d\gamma'\right\} \frac{d\tilde{\psi}}{dt}.$$ (22)

The perturbation of ψ is expressed by the following Fourier equation:

$$\tilde{\psi} = -\psi \exp(i\xi y + \lambda t),$$ (23)

where ξ is the wave number in the y direction, normal to the localized band and λ denotes the rate of the perturbation growth. Negative sign refers to the fact that the perturbation of ψ is decreased. Replacing Eq. (23) into Eq. (22) gives:

$$\frac{d\tilde{\gamma}}{dt} = \{\frac{1}{m\gamma^{n/m}}\int_0^\gamma \frac{\tau[1-R\psi^2-\mu N](\gamma')^{n/m}}{\tau(\gamma')}d\gamma'\}\exp(i\xi y+\lambda t).$$ (24)

Eq. (24) shows the retarding effect of m. The term $R\psi^2$ represents the role of m_s and n_s, which characterized the type of alloy and ψ. Considering the previous discussion on sign of R, it can be deducted that increasing ψ results in increasing the tendency of localization at low and modest strain rates. The reverse trend may be expected at very high strain rates. Moreover, according to Eq. (5b) increasing ψ results in decreasing m which promotes the localization. Moreover, inserting Eq. (23) into Eq. (21) gives:

$$\lambda = \frac{-\xi^2}{\{\frac{\beta}{\chi N \tau_s mK(\psi)(\gamma)^{n/m}}\int_0^\gamma \frac{\Lambda(\gamma')^{n/m}}{\tau(\gamma')}d\gamma'\}}.$$ (25)

The term in the parenthesis is negative, therefore $\lambda(\xi)$ acts as a high pass filter, leading smaller ξ to be filtered out relative to higher wave numbers. Consequently, the failure mode is localized rather than diffused.

4 VALIDATION OF THE MODEL

The compression test data of an A356 aluminum alloy form the work of Nguyen et al. [22] and the results of the pure shear test data of a Pb-Sn alloy from the work of Martin et al. [23] were used for validating of the model.

4.1 Validating by A356 aluminum alloy

Compression tests of an A356 aluminum alloy was performed by Nguyen et al. [20] at $584°C$, $\psi = 0.6$, with the strain rates of 0.002, 0.008 and 0.032/s. To validate the proposed constitutive equation, the initial stage of the deformation, homogeneous deformation, is considered. The necessary material parameters are listed in Table 1.

Table 1
Parameters associated with A356 alloy to verify the model.

m_{solid}	n_{solid}	K_{solid}	K_{liquid}
0.16	0.005	$60 MPa$	$2\times10^{-2} pa.s$

The low value of n is related to the fact that the strain hardening of alloy at such temperatures is almost negligible. The model predictions and the experimental results are shown in Fig. 2. It is clear that the flow curves predicted by the model are in a good agreement with the experimental data.
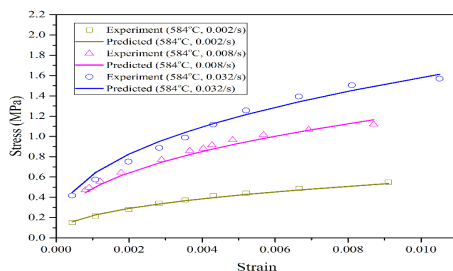
Fig.2
Stress-strain curves of the experimental results and predicted results for A356 alloy.

4.2 Validating by Pb-Sn alloy

Martin et al. [21] performed a simple shearing test on a *Pb-Sn* alloy by rheometer at three solid fractions of 0.62, 0.7 and 0.8, correspond to ψ values of 0.3, 0.42 and 0.57, respectively, with the strain rates of 0.5/*s*. The necessary *Pb-Sn* alloy parameters for validating are listed in Table 2.

Table 2
Parameters associated with *Pb-Sn* alloy to verify the model.

m_{solid}	n_{solid}	K_{solid}	K_{liquid}
0.2	0.005	$6 MPa$	$2 \times 10^{-2} \, pa.s$

The model predictions and the experimental results are shown in Fig. 3.
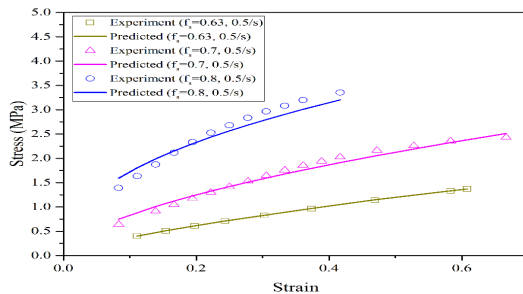
Fig.3
Stress-strain curves of the experimental results and predicted results for *Pb-Sn* alloy.

It can be observed that the predicted curves have a same trend with the experimental data, which illustrates the capability of the model to reproduce the experimental data at different values of ψ. Moreover, the curves pertain to the initial stage become linear with decreasing ψ.

5   CONCLUSIONS

In this study, the localization in the semi-solid deformation was investigated by the linear perturbation analysis on a developed viscoplastic constitutive model. The main features of the analysis are summarized as follows.
- The perturbation grows with high values of wave numbers results in a diffused failure mode instead of a localized mode.
- The perturbation analysis reveals that the localization occurs as soon as the granular deformation initiates. It necessitates the breakdown of the bonds between agglomerates.
- Decreasing the solid skeleton has a retarding effect on the perturbation growth and localization. It is attributed to the decrease in the amount of dilatancy between agglomerates.

REFERENCES

[1]   Kang C.G., Choi J.S., Kim K.H., 1999, The effect of strain rate on macroscopic behaviour in the compression forming of semi-solid aluminium alloy, *Journal of Materials Processing Technology* **88**: 159-168.
[2]   Atkinson H.V., 2005, Modelling the semisolid processing of metallic alloys, *Progress in Materials Science* **50**: 341-412.
[3]   Koeune R., Ponthot J.P., 2008, A one-phase thermomechanical constitutive model for the numerical simulation of semi-solid thixoforming, *International Journal of Material Forming* **1**: 1007-1010.
[4]   Bayoumi M.A., Negm M.I., El-Gohry A.M., 2009, Microstructure and mechanical properties of extruded Al–Si alloy (A356) in the semi-solid state, *Materials & Design* **30**: 4469-4477.
[5]   Favier V., Atkinson H.V., 2011, Micromechanical modelling of the elastic–viscoplastic response of metallic alloys under rapid compression in the semi-solid state, *Acta Materialia* **59**: 1271-1280.
[6]   Gourlay C.M., Dahle A.K., 2007, Dilatant shear bands in solidifying metals, *Nature* **445**: 70-73.

[7]   Gourlay C.M., Dahle A.K., Nagira T., Nakatsuka N., Nogita K., Uesugi K., 2011, Granular deformation mechanisms in semi-solid alloys, *Acta Materialia* **59**: 4933-4943.

[8]   Fonseca J., O'Sullivan C., Nagira T., Yasuda H., Gourlay C.M., 2013, In situ study of granular micromechanics in semi-solid carbon steels, *Acta Materialia* **61**: 4169-4179.

[9]   Kareh K.M., O'Sullivan C., Nagira T., Yasuda H., Gourlay C.M., 2017, Dilatancy in semi-solid steels at high solid fraction, *Acta Materialia* **125**: 187-195.

[10]   Meylan B., Terzi S., Gourlay C.M., Suéry M., Dahle A.K., 2010, Development of shear bands during deformation of partially solid alloys, *Scripta Materialia* **63**: 1185-1188.

[11]   Montassar S., Buhan P., 2006, Some general results on the stability and flow failure of rigid viscoplastic structures, *Mechanics Research Communications* **33**: 63-71.

[12]   Hu X.G., Zhu Q., Atkinson H.V., Lu H.X., Zhang F., Dong H.B., 2017, A time-dependent power law viscosity model and its application in modelling semi-solid die casting of 319s alloy, *Acta Materialia* **124**: 410-420.

[13]   Rudnicki J.W., Rice J.R.,1975, Conditions for the localization of deformation in pressure-sensitive dilatant materials, *Journal of the Mechanics and Physics of Solids* **23**: 371-394.

[14]   Vardoulakis I., 1977, Sensitivity analysis of the shear band bifurcation solution in the biaxial test on sand samples, *Mechanics Research Communications* **4**: 171-177.

[15]   Bai Y.L., 1982, Thermo-plastic instability in simple shear, *Journal of the Mechanics and Physics of Solids* **30**: 195-207.

[16]   Anand L., 1987, Onset of shear localization in viscoplastic solids, *Journal of the Mechanics and Physics of Solids* **35**: 407-429.

[17]   Desoyer T., Hanus J.L., Keryvin V., 1998, An instability condition of the deformation process in elasto-(visco)-non-linear materials, *Mechanics Research Communications* **25**: 437-442.

[18]   Aghaie-Khafri M., Mahmudi R., 2005, The effect of preheating on the formability of an Al–Fe–Si alloy sheet, *Journal of Material Processing and Technology* **169**: 38-43.

[19]   Aghaie-Khafri M., Mahmudi R., 2005, Optimizing homogenization parameters for better stretch formability in an Al-Mn-Mg alloy sheet, *Materials Science and Engineering A* **399**: 173-180.

[20]   Sheikh-Ansari M.H., Aghaie-Khafri M., 2017, Predicting flow localization in semi-solid deformation, *International Journal of Material Forming* **11**: 165-173.

[21]   Terzaghi K.V., 1936, The shearing resistance of saturated soils, *Proc 1st ICSMFE* **1**: 54-56.

[22]   Nguyen T.G., Favier D., Suery M., 1994, Theoretical and experimental study of the isothermal mechanical behaviour of alloys in the semi-solid state, *International Journal of Plasticity* **10**: 663-693.

[23]   Martin C.L., Brown S.B., Favier D., Suéry M., 1995, Shear deformation of high solid fraction (>0.60) semi-solid Sn-Pb under various structures, *Materials Science and Engineering: A* **202**: 112-122.